Asian Journal of Chemistry; Vol. 33, No. 8 (2021), 1796-1804

ASIAN JOURNAL OF CHEMISTRY

https://doi.org/10.14233/ajchem.2021.23254

Synthesis, Crystal Structure, Hirshfeld, DFT, Quorum Sensing Inhibition and Molecular Docking Studies of *N'*-{(*E*)-[3-(3,5-Difluorophenyl)1*H*-pyrazol-4-yl]methylidene}-4-methoxybenzohydrazide

VASANTHA KUMAR[1,*], D. GANAVI[2,3], B. SUKESH KUMAR[4], RAJESH P. SHASTRY[4], A.H. UDAYA KUMAR[5], S. MADAN KUMAR[6], MOHAMMED AL-GHORBANI[7,8], P.M. GURUBASAVARAJA SWAMY[9], N.K. LOKANATH[5], K. NAVEEN[1] and BOJA POOJARY[3]

[1]Department of P.G. Chemistry, Sri Dharmasthala Manjunatheshwara College (Autonomous), Ujire-574240, India
[2]Department of Chemistry, Sri Dharmasthala Manjunatheshwara College (Autonomous), Ujire-574240, India
[3]Department of Studies and Research in Chemistry, Mangalore University, Mangalagangotri-574199, India
[4]Yenepoya Research Centre, Yenepoya (Deemed to be University), University Road, Mangalore-575018, India
[5]Department of Studies in Physics, University of Mysore, Manasagangotri, Mysuru-570006, India
[6]IOE, University of Mysore, Manasagangotri, Mysuru-570 006, India
[7]Department of Chemistry, Thamar University, Dhamar, Yemen
[8]Department of Chemistry, Science and Arts College, Ulla, Taibah University, Madinah, Saudi Arabia
[9]Department of Pharmaceutical Chemistry, Acharya & B.M. Reddy College of Pharmacy, Soldevanahalli, Bangalore-560107, India

*Corresponding author: E-mail: vasantha.kumar1886@gmail.com

Received: 20 April 2021; *Accepted*: 12 May 2021; *Published online*: 26 July 2021; AJC-20430

In present study, the synthesis, structural, quorum sensing inhibition and computational studies of a new *N'*-{(*E*)-[3-(3,5-difluorophenyl)-1*H*-pyrazol-4-yl]methylidene}-4-methoxybenzohydrazide are reported. The structure of the synthesized compound was confirmed by IR, ^{1}H & ^{13}C NMR and mass spectral data. The single crystals of the compound was obtained using ethanol as a crystallization solvent. The synthesized compound ($C_{40}H_{40}N_8O_6F_4$) crystallizes in the monoclinic crystal system, *C*2/*c* space group. Various intermolecular interactions were quantified using a 3D molecular Hirshfeld surface computational method. The 2D fingerprint plots revealed that the H···H (35.9%) interactions have a major contribution to the total molecular surface. DFT studies was performed to establish the molecular crystal structure of the compound and to study the HOMO-LUMO energies of the compound. The anti-quorum sensing study of the target compound on *Chromobacterium violaceum* (wild type) biosensor revealed that quorum quenching activity at 300 µg/mL. Interestingly, quantitative assay exhibited more than 80% of quorum sensing inhibition without interfering cell growth ($p < 0.05$). Molecular docking studies of the compound on CviR protein (PDB: 3QP8) confirmed the observed activity through strong hydrogen bonding interaction with the amino acids in the binding pocket.

Keywords: Pyrazole, Hydrazone, Crystal study, Hirshfeld study, Quorum sensing inhibition, Molecular docking studies.

INTRODUCTION

Pyrazole class of compounds are one of the main groups of heterocyclic molecules possessing a wide range of applications in various areas of medicinal and material chemistry. Pyrazole ring is an important structural moiety found in innumerous pharmaceutically active compounds [1]. In recent years, pyrazole derivatives exhibit a wide range of biological activities [2] such as antimicrobial [3], anti-inflammatory [4], anticancer [5], antimalarial agents [6], fungicidal [7] and antiviral [8] activities. Meanwhile, hydrazones are compounds having the basic structure $R_1R_2C{=}NNH_2$. These are important intermediates in the heterocyclic chemistry. Hydrazones are well documented in literature as a framework of organic compounds with tremendous potential as a target for various biological activities [9]. They are used as pigments, dyes, intermediates in organic synthesis and as polymer stabilizers [10]. Hydrazones have also been shown to exhibit a broad range of biological activities, including antimicrobial [11], antimalarial [12], antiproliferative [13], anti-inflammatory [14], antiviral [15], analgesic [16], antidiabetic [17] and antihypertensive [18]. It is also worth to mention several pyrazole embedded hydra-

zones also possess various biological activities such as antibacterial [19], antifungal [20], anticancer [21], anticonvulsant [22], anti-inflammatory [23] and antiplatelet activities [24].

Since the early 20th century, antibiotics have been the primary drugs against infections [25]. However, with the continued emergence of superbugs and untreatable infections, antibiotic resistance may become a leading concern [26]. Moreover, antimicrobial agents against classical targets and involving conventional screening methods cannot fundamentally address this concern. Identifying new targets and developing antimicrobial agents with new action mechanisms are urgent [27]. Quorum sensing (QS) is a bacterial communication process that relies on extracellular signalling molecules called autoinducers [28]. Quorum sensing regulates the survival and pathogenicity of bacteria [29], which has attracted the attention of pharmacologists and has made QS an important target for new antibacterial drug development [30]. These QS inhibitors, instead of killing bacteria or inhibiting their growth, quench QS-regulated pathogenic behaviours, such as toxin production, biofilm formation, swarming and secretions, which cause bacteria to lose their ability to cause a disease and to induce drug resistance [28]. This action mechanism of antimicrobial agents is greatly different from traditional antibiotics. Therefore, QS-targeted antimicrobial drugs are regarded ideal antibacterial drugs of future [31].

Based on these observations and in continuation of our work on quorum sensing inhibition [32,33] and pyrazole derivatives [34,35], in the present study, *N′*-{(*E*)-[3-(3,5-difluorophenyl)-1*H*-pyrazol-4-yl]methylidene}-4-methoxy-benzohydrazide was synthesized and its structure was confirmed by single crystal data. Molecular interactions are quantified by Hirshfeld surface analysis. DFT calculations were performed to optimize the structure of the molecule with the obtained crystal structure of the molecule. Further, target molecule was screened for its quorum sensing inhibition on *Chromobacterium violaceum* (wild type) biosensor. Molecular docking studies were performed to understand plausible mode of action of a compound through its binding interaction with CviR protein (PDB 3QP8).

EXPERIMENTAL

Starting materials were purchased from Sigma-Aldrich (India) and used as such. All the solvents and reagents were purchased from the commercial vendors in the appropriate grade and used without purification. Melting points were determined by an open capillary method and are uncorrected. FTIR spectra were recorded on KBr pellets using Perkin-Elmer spectrum 1000 spectrometer. ^{1}H & ^{13}C NMR spectra were recorded on BRUKER AVANCE II-300 (400 MHz and 100 MHz) spectrometer using TMS as an internal standard. Mass spectra were recorded in Agilent Technology LC-Mass spectrometer. The elemental analysis was carried out using CHNS Elemental Vario EL III. The progress of the reaction was monitored by thin layer chromatography (TLC) on a silica coated aluminium sheet (silica gel 60F_{254}).

Synthesis of (*E*)-*N′*-((3-(3,5-difluorophenyl)-1*H*-pyrazol-4-yl)methylene)-4-methoxybenzohydrazide (3): To a mixture of 4-methoxybenzohydrazide (**1**) (0.199 g, 0.0012 mol) and 3-(3,5-difluorophenyl)-1*H*-pyrazole-4-carbaldehyde (**2**) (0.25 g, 0.0012 mol) in absolute ethanol, added catalytic amount of glacial acetic acid. The reaction mixture was refluxed for 8 h. After the completion of the reaction (TLC ethyl acetate:hexane; 3:7), the reaction mass was cooled to room temperature. Solid precipitate was filtered, washed with water and dried. The compound was recrystallized by ethanol. Yield: 84%; m.p.: 123-125 ºC; FTIR (KBr, ν_{max}, cm^{-1}): 3231 (N-H), 3086, 3020 (=C-H), 2934, 2839 (C-H), 1646 (C=O), 1608 (C=N), 1548 (C=C), 1372 (C-O), 1175 (C-F); ^{1}H NMR (400 MHz, DMSO-d_6, δ ppm): 13.56 (s, 1H, pyrazole-NH), 11.57 (s, 1H, O=C-NH), 8.58 (s, 1H, pyrazole-CH), 8.20 (s, 1H, CH=N), 7.90 (2H, d, Ar-$H_{m\text{-}OMe}$, J = 8.8 Hz), 7.46 (s, 2H, Ar-$H_{o\text{-}F}$), 7.28 (s, 1H, Ar-$H_{o\text{-}F}$), 7.O4 (d, 2H, Ar-$H_{o\text{-}OMe}$, J = 8.4 Hz), 3.82 (s, 3H, OCH_3); ^{13}C NMR ($CDCl_3$, 400 MHz, δ ppm): 168.9, 168.8 and 166.5, 166.4 (Ar-C_F), 167.4 (C=O), 167.0 (Ar-C_{OMe}), 152.6, 145.8, 141.8, 136.6, 134.6, 130.8, 119.8, 118.8, 116.5, 116.2, 108.4, 60.5 (-OCH_3); LCMS (*m/z*): 357.32 (M^++H).

X-ray diffraction studies: Defect free white coloured single crystal of dimension 0.40 mm × 0.32 mm × 0.33 mm of the compound **3** was selected for the intensity data collection at a temperature 296.15 K on a Bruker Proteum2 CCD diffractometer equipped with an X-ray generator operating at 45 kV and 10 mA, using Cu*K*α radiation of wavelength 1.54178 Å. Data were collected for 24 frames per set with different φ (0º and 90º), keeping the scan width of 0.5°, exposure time of 1.2 s, the sample to detector distance of 50 mm and 2θ value at 46.6º. The complete data were processed using SAINT PLUS [36]. All the frames could be indexed by using a monoclinic crystal system in the *C*2/*c* space group and the crystal structure was solved by using the direct method and refined by the full least squire method on F^2 using SHELXS and SHELXL [37]. All the non-hydrogen atoms were anisotropically refined and the hydrogen atoms were positioned geometrically and refined using a riding model with Uiso(H) = 1.2 Ueq and 1.5 Ueq. Parameters are refined with 2396 unique reflections of 16009 observed reflections. After several cycles of refinement, the final difference Fourier map showed peaks of no chemical significance and the residual is saturated to 0.0391. The geometric calculations are carried out using the program PLATON [38]. The visualization of the molecular and packing diagram was generated using the CCDC software MERCURY [39].

Hirshfeld analysis: The crystallographic information file (cif) used to estimate the molecular pair wise model energies between the molecule within the standard cluster of a radius of 3.8 Å at the B3LYP/6-31G (d,p) basis set by Crystal Explorer 17.5 [40]. 3D molecular Hirshfeld surface and 2D fingerprint plots were produced using the standard value 0.6 to 2.6 Å to represent the d_i and d_e values in the graph. The total interaction energy is the sum of classical electrostatic energy (E_{ele}), exchange-repulsion energy (E_{rep}), polarization energy (E_{pol}) and dispersion energy (E_{dis}), between the molecules of the cluster. The calculated energies are represented through the construction of energy frameworks and the size of the tube indicates the strength of the interaction energy [41-43].

DFT studies: The density functional theory (DFT) computation has been executed for the compound **3** using Gaussian 16W package [44]. The molecular structure is used to generate optimized geometry using crystal structure coordinates (CIF) as input, in B3LYP/6-311+G(d,p) [45] hybrid level basis set without any constraints. Further, vibrational frequency calculation was carried out to confirm whether the optimized structure is at the minima point on the potential energy surface. The Khon-Sham frontier molecular orbitals, molecular electrostatic potential map (MEP) and ground state energy of compound **3** are extracted from the optimized geometry. HOMO, LUMO, energy gap and related global reactive parameters (electronegativity, hardness, softness and electrophilicity chemical potential) are estimated with Koopman's approximation. HOMO, LUMO and MEP are visualized through Gaussview 6.0.16 software [46].

Quorum sensing inhibition assay

Bacterial strains: *Chromobacterium violaceum* ATCC 12427 (provided by Robert McLean) used as biosensor for anti-quorum sensing studies. *C. violaceum* was maintained in Luria-Bertani (LB) broth at 30 ºC in a rotary shaker incubator for 24 h.

Anti-quorum sensing activity: The quorum sensing inhibition (QSI) assay was performed as reported method with some modification [47]. Briefly, the sterile paper disc was loaded with compound **3** and placed into *C. violaceum* (overnight culture) pre-seeded LB agar plates. The plates were incubated at 30 ºC for 24 h. After the incubation time, the plates were observed around the discs for the presence of a clear zone (inhibition of violacein production). The presence of a clear zone suggests that the inhibition of quorum sensing in *C. violaceum* biosensor strain. Vanillin (Himedia, India) was used as a standard QSI molecule [48].

Quantification of anti-quorum sensing activity: The QSI of compound **3** was quantified as reported method [49,50] Briefly, the 24 h grown culture of *C. violaceum* inoculated to LB medium along with compound **3** in 10 mL culture tube in triplicates. The culture tubes were incubated for 24 h at 30 ºC. After the incubation time, 1 mL of *C. violaceum* culture from each tube (treated with QSI) was transferred to a microcentrifuge tube. Then, it was centrifuged at 10000 rpm for 5 min. The supernatant was removed and the cell pellet equal volume of DMSO was added. It was vortexed for 1 to 2 min and centrifuged at 10000 rpm for 5 min to remove the cells. The violacein containing supernatants were transferred (200 µL) to 96-well microplates and the absorbance was read with a microplate reader at a wavelength of 585 nm. The harvested bacterial cell growth was measured at 600 nm by resuspending in1 mL of sterile water. The results were compared with respective assay control (without compound).

Molecular docking study: Molecular docking for compound **3** was carried out on CviR (*Chromobacterium violaceum*) protein (PDB 3QP8). Docking was performed using Drug Discovery Studio 3.5. The required structure of proteins, as well as compound **3**, was prepared. The prepared proteins were defined as a receptor molecule by clicking on define selected molecule as receptor under define and edit the binding site and by selecting only the ligand part and clicking on define sphere from receptor site. The prepared receptor input into the receptor molecule parameter in the CDOCKER protocol parameter explorer. Each molecule was given as input in other parameters meant for input ligands and the protocol was run. The CDOCKER ENERGY of best poses docked into the receptor of the target compound was calculated.

Statistical analysis: Statistical significance of variance for quantification of the quorum sensing inhibition activity was analyzed by one-way ANOVA followed by Tukeys test. Statistical analyses were performed using Graphpad Prism 5.03 software.

RESULTS AND DISCUSSION

The synthesis of *N*′-{(*E*)-[3-(3,5-difluorophenyl)-1*H*-pyrazol-4-yl]methylidene}-4-methoxybenzohydrazide (**3**) is depicted in **Scheme-I**. The target compound was synthesized by the reaction of acid hydrazide (**1**) with 3-(3,5-difluorophenyl)-1*H*-pyrazole-4-carbaldehyde (**2**) in the presence of a catalytic amount of glacial acetic acid in ethanolic medium. The structure of the final compound was confirmed by IR, ^{1}H NMR, ^{13}C NMR and LCMS data.

Formation of *N*′-{(*E*)-[3-(3,5-difluorophenyl)-1*H*-pyrazol-4-yl]methylidene}-4-methoxybenzohydrazide (**3**) was confirmed by the presence of N-H band at 3231 cm^{-1} and carbonyl stretching band 1645 cm^{-1}. It showed C-F stretching band at 1175 cm^{-1}. Its ^{1}H NMR spectrum showed a singlet at δ 8.28 ppm for the imine proton indicating the formation of a product. The pyrazole N-H and N-H of hydrazone appeared as two distinct singlets at 13.56 ppm and 11.58 ppm, respectively. The pyrazole C-H resonated as a singlet at 8.58 ppm. Three protons of 3,5-diflourophenyl ring appeared as two singlets at 7.46 ppm and 7.29 ppm, respectively. The protons *meta* and *ortho* to the methoxy group of 4-methoxyphenyl ring resonated as two distinct doublets centered at 7.90 ppm and 7.04 ppm respectively. In its ^{13}C spectrum, it showed a signal at δ 167.1 ppm corresponding to the C=O of carbohydrazone. The fluorine-

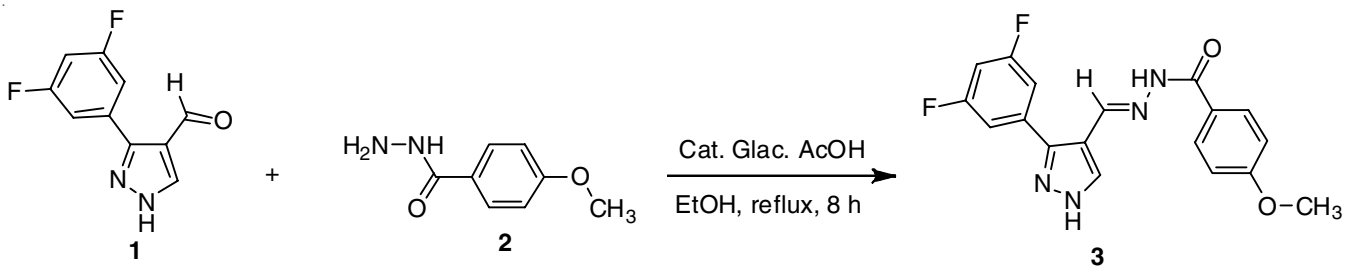

Scheme-I: Synthesis of (*E*)-*N*'-((3-(3,5-difluorophenyl)-1*H*-pyrazol-4-yl)methylene)-4-methoxybenzohydrazide (**3**)

carbon coupling was observed in the target molecule which shows a $^{1}J_{F\text{-}C}$ coupling to give doublet centered at 167.67 ppm with J = 244 Hz and this doublet will further split into a doublet of doublets ($^{3}J_{F\text{-}C}$) with J = 13 Hz. It displayed a signal for the carbons present at *meta* and *ortho* to the methoxy group at δ 134.6 ppm and δ 118.8 ppm, respectively. Methoxy carbon of aromatic hydrazide moiety appeared at δ 60.5 ppm. Further, its mass spectrum showed a protonated molecular ion peak at 357.32 in confirmation with the molecular formula $C_{18}H_{14}N_4O_2F_2$.

Single crystal XRD: Single crystal XRD analysis revealed that the compound **3** ($C_{40}H_{40}N_8O_6F_4$) is crystallized in the monoclinic crystal system, *C*2/*c* with a lattice solvent (ethanol) in the asymmetric unit. The unit cell parameter are a = 27.1368 (19) Å, b = 7.9323(6) Å, c = 18.5985(13) Å, β = 102.288(2)º and unit cell volume 3911.7(5) Å^3 with Z = 4. Fig. 1 shows the ORTEP view of compound **3** with thermal ellipsoidal drawn at 50% probability and Table-1 depicts the crystal structure refinement data compound **3**. The molecular structure consists of benzene ring with functional group OCH_3 is slightly deviated from the pyrazole ring about dihedral angle of 21.41º, whereas 3,5-dichlorophenyl ring is twisted about dihedral angle of 47.12º which makes the molecule non-planar. The crystal structure is stabilized by several types of strong intra and intermolecular hydrogen bonding interactions. The potential hydrogen bonds of the title compound are enlisted in Table-2 with symmetry code. The packing of the molecules along the crystallographic *b*-axis, the dotted line s indicating the hydrogen bond interaction between the nitrogen atom of the pyrazole ring and carbonyl oxygen group forms $R_2^2(18)$ supramolecular synthon. The C-H···F interaction rendered through hydrogen and fluorine of phenyl ring forms $R_2^2(8)$ ring motif interconnects linear 1D chain to construct the 2D planar sheet is depicted in Fig. 2.

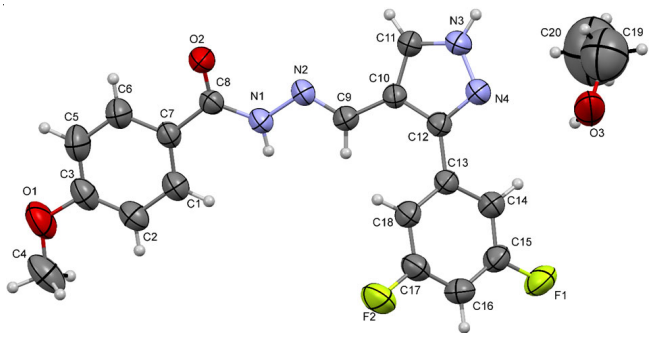

Fig. 1. ORTEP of compound **3** with the thermal ellipsoids are drawn at 50% probability

TABLE-1
CRYSTAL STRUCTURE DATA AND REFINEMENT DETAILS OF COMPOUND **3**

CCDC deposit No.	2070046
Empirical formula	$C_{40}H_{40}F_4N_8O_6$
Formula weight	804.80
Temperature (K)	296.15
Wavelength (Å)	1.54178
Crystal system, space group	Monoclinic, *C*2/*c*
Unit cell dimensions	
a	27.1368(19) Å
b	7.9323(6) Å
c	18.5985(13) Å
β	102.288(2)°
Volume Å^3	3911.7(5)
Z	4
Density (calculated) (g cm^{-3})	1.367
Absorption coefficient (mm^{-1})	0.902
F_{000}	1680.0
Crystal size (mm)	0.40x0.32x0.33
θ range for data collection	12.898º to 109.726º
Index ranges	-25 ≤ h ≤ 28; -8 ≤ k ≤ 8; -19 ≤ l ≤ 18
Reflections collected	16009
Independent reflections	2396 [R_{int} = 0.0391]
Refinement method	Full matrix least-squares on F^2
Data/restraints/parameters	2396/174/269
Goodness-of-fit on F^2	1.055
Final [I >2σ(I)]	R1 = 0.0657, wR2 = 0.1878
R indices (all data)	R1 = 0.0680, wR2 = 0.1904
Largest diff. peak and hole	0.53 and -0.38e Å^3

TABLE-2
POTENTIAL HYDROGEN BOND INTERACTIONS IN COMPOUND **3**

D–H···A (Å)	D-H (Å)		H···A (Å)	D–H···A (°)
N1-H1A···O3$^{(i)}$	0.85(3)	2.24	2.24(3)	167(3)
N3-H3···O2$^{(ii)}$	0.86	1.99	2.820(3)	162
C1-H1A···O3$^{(i)}$	0.93	2.49	3.416(4)	173
C4-H4A···F1$^{(iii)}$	0.96	2.49	3.417(5)	166
C9-H9A···O3$^{(i)}$	0.93	2.49	3.340(4)	152
C19-H19A···O2$^{(ii)}$	0.97	2.59	3.524(9)	161

(i) 3/2-*x* -1/2+*y*,3/2-*z*, (ii) 3/2-*x*,3/2-*y*,1-*z*, (iii)-1/2+*x*,1/2-*y*,-1/2+*z*

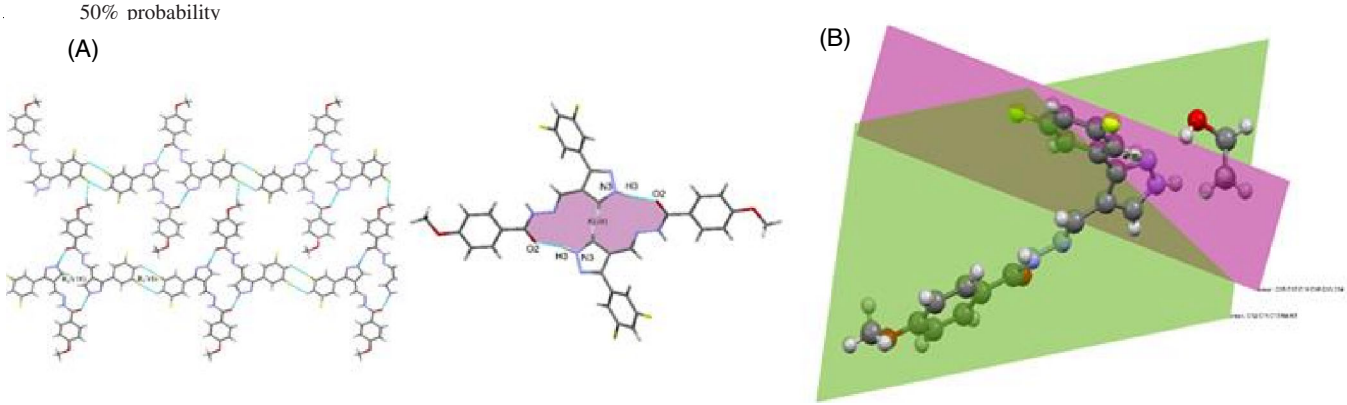

Fig. 2. (A). Packing of the molecules when viewed along b' axis. The dotted lines indicate the intermolecular hydrogen bond and short interactions and (B). Non-linearity representation of the compound **3**

Hirshfeld surface analysis: In 3D molecular Hirshfeld surface analysis of compound **3**, the d_{norm} surface mapped over colour scale -0.22(red) to 1.4 Å (blue) and red colour spots show the dominance of O...H and H...O hydrogen bond interaction while blue colour indicates the long and weak contact shown Fig. 3. The 3D picture of the close contacts shown in the figure is summarized in a 2D fingerprint plot. The largest contributor to the total surface is H···H (35.9%) contact and other significant contacts to the total molecular Hirshfeld surface is shown in Fig. 4.

The detailed interaction energies between the molecules of a cluster are resolved into classical electrostatic (E_{ele}), polarization (E_{pol}), dispersion (E_{dis}) and repulsion (E_{rep}) components. The net interaction energy of compound **3** is E_{tot} = -402.5 kJ/mol with the combination of $E_{el\,e}$ = -253.47 kJ/mol, E_{pol} = -61.93 kJ/mol, E_{dis} = -333.85 kJ/mol and E_{rep} = 246.767 kJ/mol. The topological representation of the above energy values along the *b*-axis is visualized through the energy frameworks (Fig. 5).

DFT studies: Quantum chemical calculations indicate that the optimized structure is in good agreement with the crystal structure of compound **3**. The ground state of the optimized structure is -1418.88 Hartree. The frontier molecular orbitals are depicted with an energy gap 4.163 eV is shown in Fig. 6. The HOMO and LUMO are delocalized throughout the skeleton of compound **3** and not on the lattice solvent. The hardness, softness, electronegativity, chemical potential and the electrophilicity values of compound **3** is given in Table-3.

The MEP 3D plot (Fig. 7) reflects the electrophilic and nucleophilic active sites and provides the information of hydrogen bond contacts based on the electron density of the compound **3**. The MEP generated with the different colour scale range (red < orange < yellow < green) indicates electronegativity

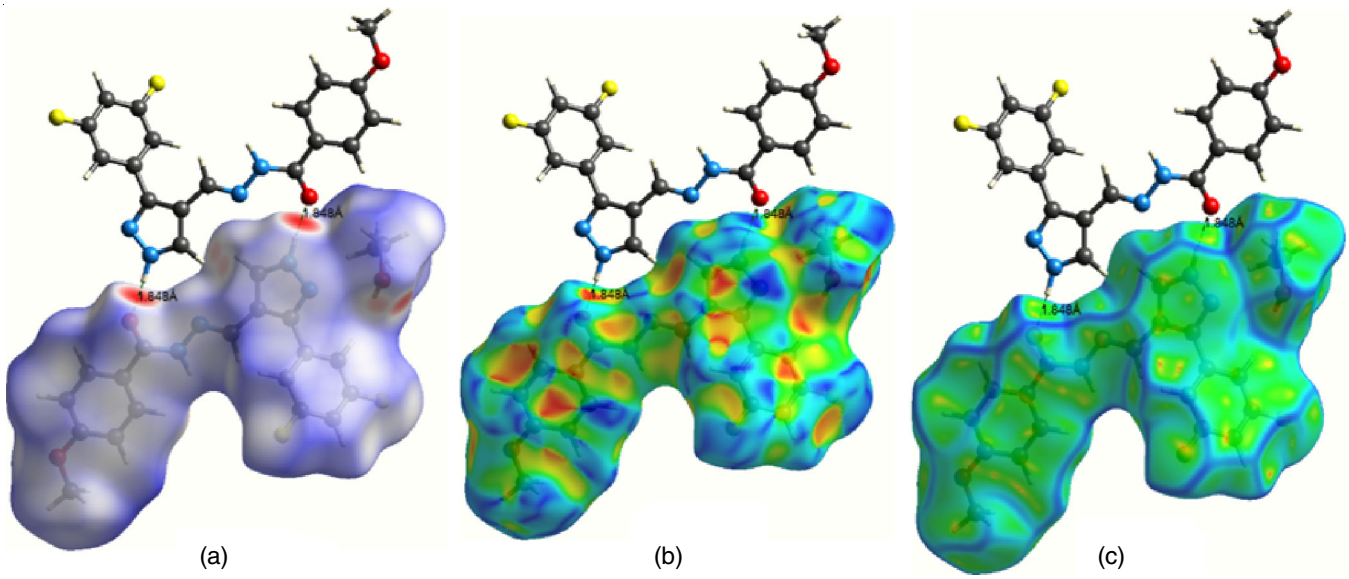

Fig. 3. d_{norm} (a) shape index (b) curvedness (c) mapped on Hirshfeld surface of the compound **3**

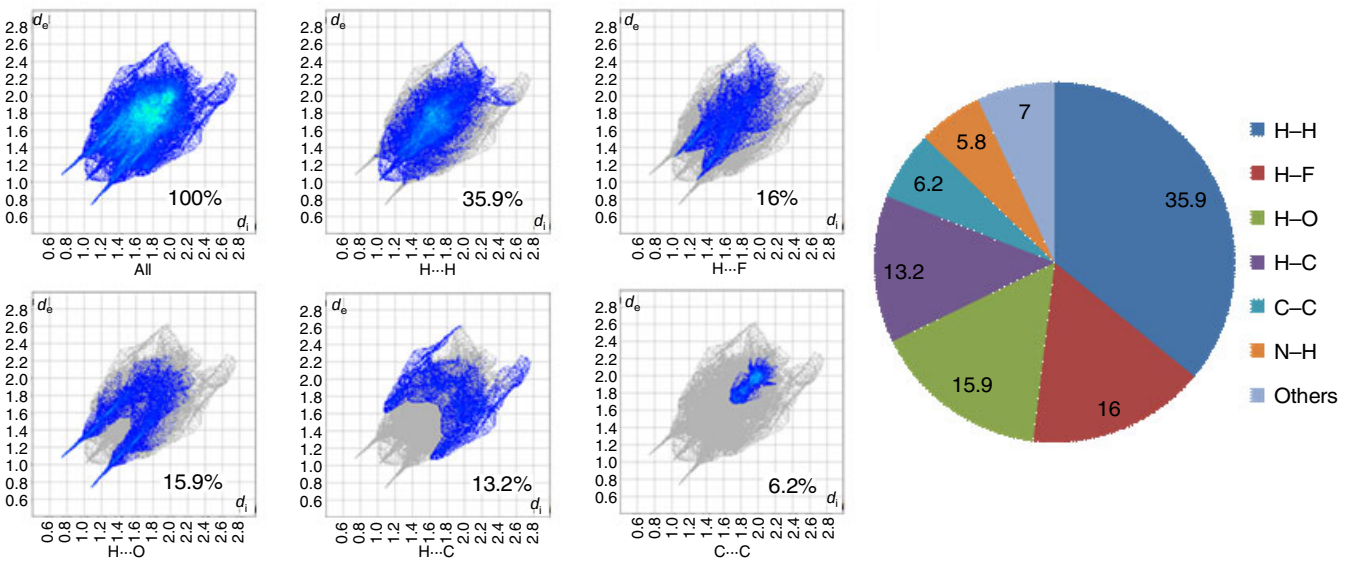

Fig. 4. 2D fingerprint plots of compound **3**. d_i is the closest internal distance from a given point on the Hirshfeld surface and d_e is the closest external contacts. The outline of the full fingerprint is shown in gray

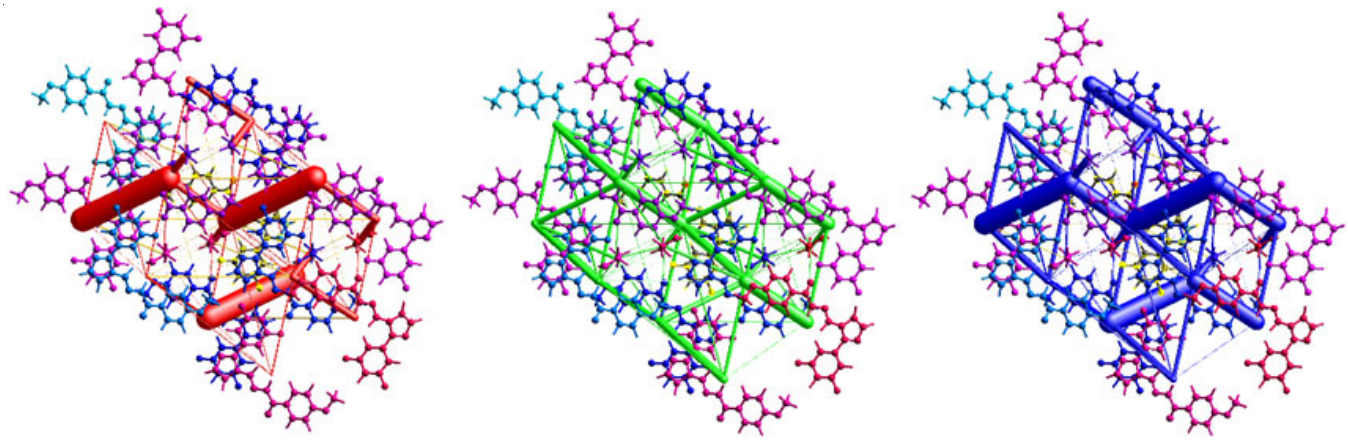

Fig. 5. Energy frameworks corresponding to electrostatic (red), dispersion (green) and total energy (blue) components of compound **3** viewed along the *b*-axis

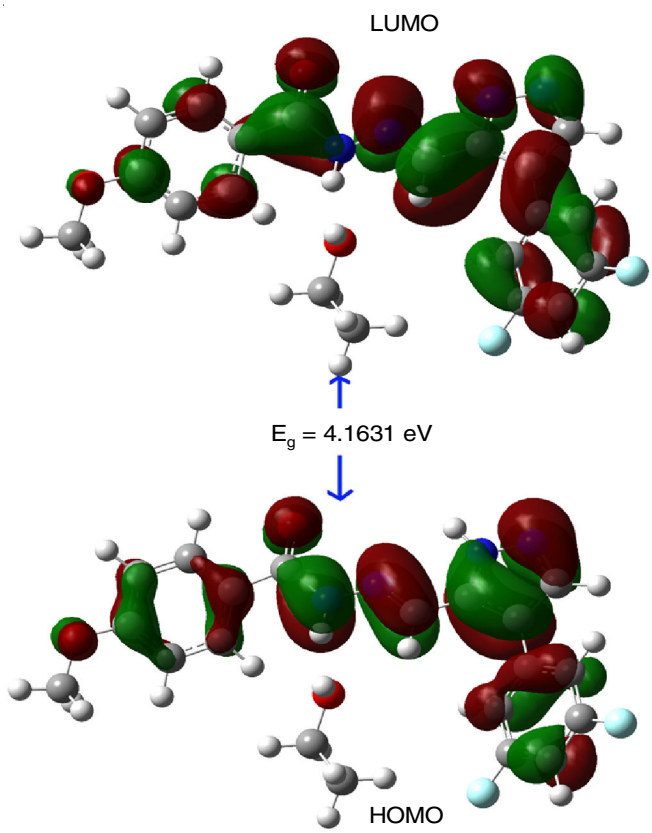

Fig. 6. Computed frontier molecular orbital of compound **3** with energy gap

TABLE-3
ENERGY VALUES AND GLOBAL REACTIVE PARAMETER OF THE OPTIMIZED STRUCTURE **3**

Parameter	Values
E_{HOMO}	-6.168
E_{LUMO}	-1.998
Energy gap (eV)	4.163
Ionization energy (eV)	6.168
Electron affinity (eV)	1.998
Electronegativity (eV)	4.083
Chemical potential (eV)	-4.083
Global hardness (eV)	2.081
Global softness (eV^{-1})	0.480
Electrophilicity index (eV)	4.001

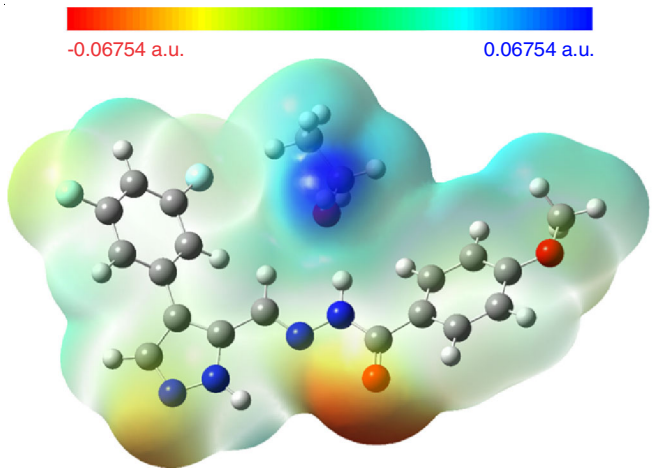

Fig. 7. Graphical view of the 3D molecular electrostatic potential (MEP) map of compound **3**

and electro positivity. The dark red colour concentrated mainly on C=O oxygen having a value of -0.06745 a.u. The dark blue colour is mainly present on lattice solvent (OH group) having 0.06745 a.u. and tend to form intermolecular contact with the nitrogen of the pyrazole ring. Hence by using MEP results, it is predicted where the structure interacts with adjacent molecules in the crystal structure [51,52].

Quorum sensing inhibition: The preliminary screening for quorum sensing inhibition potential of target compound **3** was carried out through the disc diffusion assay. *C. violaceum* was used as a biosensor to understand the inhibition of quorum sensing. Compound **3** was able to inhibit quorum sensing significantly at 300 µg/mL (Fig. 8B) and comparable with vanillin (Fig. 8C). Furthermore, to confirm this effect on cell growth, the bacterial cells were allowed to grow in the presence and absence of QS inhibitors. Then, the violacein produced was quantified by dissolving in DMSO and cell pellets were considered for growth measurement. The results revealed that compound **3** was able to inhibit quorum sensing more than 80% (Fig. 8C) at $p \geq 0.05$ suggesting the anti-QS potentiality of this molecule. Moreover, the quantification of cell growth exhibited without/negligible activity on bacterial cells suggesting that an optimum concentration for the anti-QS activity. The vanillin inhibited

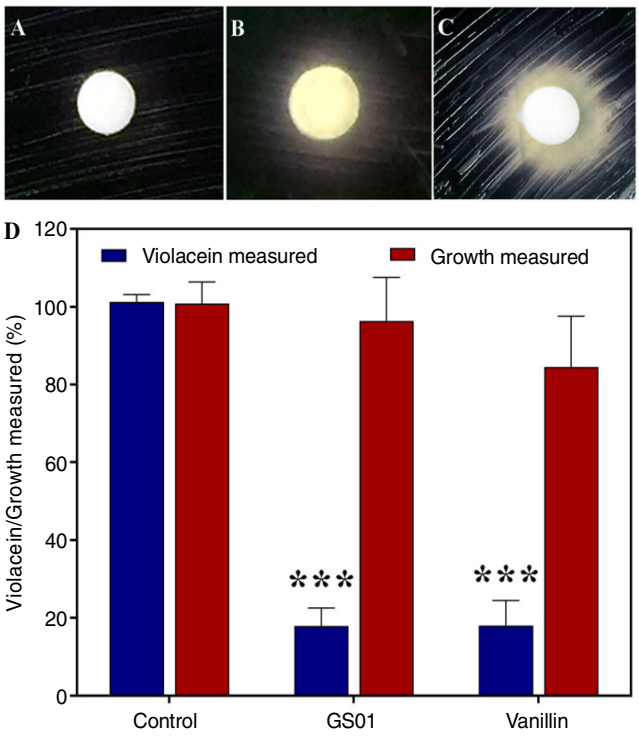

Fig. 8. Quorum quenching activity of compound **3** against *C. violaceum* biosensor strain by disc diffusion (insert, control (A), treated with compound **3** (B), Vanillin (Standard QSI) (C) and quantification method (D). The zone of violacein inhibition around the disc (B) suggests that quorum quenching activity. The quantification assay showed that inhibition of quorum sensing more than 80% at $p < 0.05$ (D)

violacein production significantly ($p \geq 0.05$), but quantification of violacein showed more than 20% inhibition of growth. Therefore, based on these results, compound **3** found to be a promising molecule to control quorum sensing in *C. violaceum*.

Molecular docking studies: A molecular docking study was performed to know the binding interaction of compound **3** with CviR (*Chromobacterium violaceum*) protein (PDB 3QP8). The docking poses (2D and 3D) of compound **3** are depicted in Fig. 9. Compound **3** binds well in the active pocket of the *C. violaceum* protein. The C-Docker energy and C-Docker interaction energy of the compound **3** is -4.88 kcal/mol and -39.055 kcal/mol, respectively. The carbonyl oxygen of 4-methoxyphenyl unit forms two hydrogen bonds with the NH_2 of GLN20 at a distance of 2.60 Å and 2.73 Å. The N-H of hydrazone involves hydrogen bonding with GLU73 at a distance of 2.79 Å. The nitrogen of the pyrazole unit forms hydrogen bonding with ARG71 at a distance of 2.35 Å. These three hydrogen bonds holds the molecule well within the active pocket of the protein. In addition to these, compound **3** also involves in π-alkyl and π-cation interactions with active site residues which accounts for the observed activity.

Conclusion

Herein, the synthesis of a novel *N*′-{(*E*)-[3-(3,5-difluorophenyl)-1*H*-pyrazol-4-yl]methylidene}-4-methoxybenzohydrazide and anti-quorum sensing inhibition studies against *Chromobacterium violaceum* biosensor strain has been described. The structure of the novel compound was confirmed by spectroscopic and single crystal XRD studies. A single crystal study revealed that the molecule crystallized in monoclinic crystal system with *C*2/*c* space group. Hirshfeld 2-D fingerprint plots revealed that the H···H (35.9%) interactions have a major contribution to the total molecular surface. The anti-quorum sensing and quantification study revealed that the compound emerged as promising with 80% inhibition and emerged as a promising molecule. Molecular docking studies depicted excellent fitting of the molecule through hydrogen bonding with GLN20, GLU73 and ARG71 residues in the binding pocket of *C.*

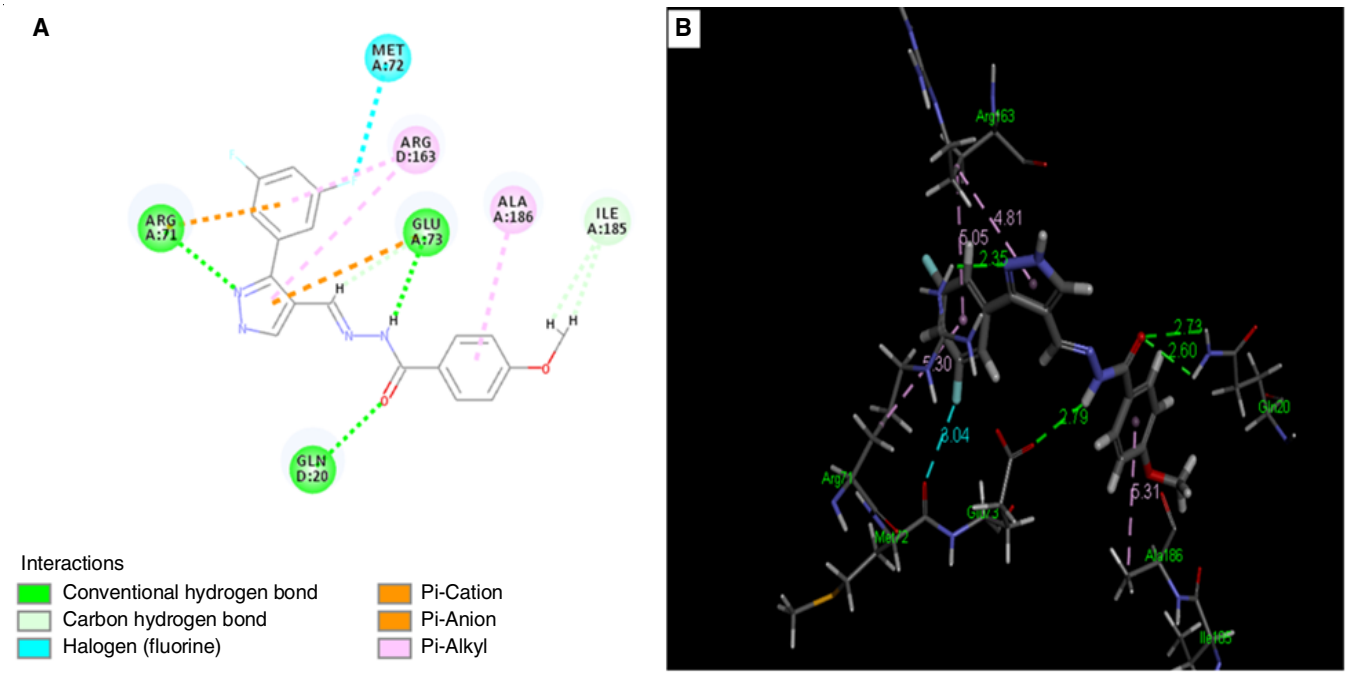

Fig. 9. The docking poses (A-2D and B-3D) of the compound **3** with CviR (*C. violaceum*) protein (PDB 3QP8)

violaceum protein. Further optimization of the core moiety is in a process to identify highly potent quorum sensing inhibitor.

ACKNOWLEDGEMENTS

One of the authors, RPS is thankful to Prof. Robert McLean, Department of Biology, Texas State University, for the gift of *C. violaceum* ATCC 12427. The authors are thankful to IOE and DST-PURSE, University of Mysore, Mysore, India for financial support.

CONFLICT OF INTEREST

The authors declare that there is no conflict of interests regarding the publication of this article.

REFERENCES

1. K. Karrouchi, S. Radi, Y. Ramli, J. Taoufik, Y.N. Mabkhot, F.A. Al-Aizari and M. Ansar, *Molecules*, **23**, 134 (2018); https://doi.org/10.3390/molecules23010134
2. Y. Mabkhot, N. Kaal, S. Alterary, S. Al-Showiman, A. Barakat, H. Ghabbour and W. Frey, *Molecules*, **20**, 8712 (2015); https://doi.org/10.3390/molecules20058712
3. R. Prasath, P. Bhavana, S. Sarveswari, S.W. Ng and E.R.T. Tiekink, *J. Mol. Struct.*, **1081**, 201 (2015); https://doi.org/10.1016/j.molstruc.2014.10.026
4. P.K. Sharma, S. Kumar, P. Kumar, P. Kaushik, D. Kaushik, Y. Dhingra and K.R. Aneja, *Eur. J. Med. Chem.*, **45**, 2650 (2010); https://doi.org/10.1016/j.ejmech.2010.01.059
5. S.M. Abu Bakr, S.S. Abd El-Karim, M.M. Said and M.M. Youns, *Res. Chem. Intermed.*, **2**, 1387 (2016); https://doi.org/10.1007/s11164-015-2091-5
6. A.A. Bekhit, A. Hymete, H. Asfaw and A.E.-D.A. Bekhit, *Arch. Pharm.*, **345**, 147 (2012); https://doi.org/10.1002/ardp.201100078
7. S. Du, Z. Tian, D. Yang, X. Li, H. Li, C. Jia, C. Che, M. Wang and Z. Qin, *Molecules*, **20**, 8395 (2015); https://doi.org/10.3390/molecules20058395
8. Z. Yang, P. Li and X. Gan, *Molecules*, **23**, 1798 (2018); https://doi.org/10.3390/molecules23071798
9. S. Rollas and S.G. Küçükgüzel, *Molecules*, **12**, 1910 (2007); https://doi.org/10.3390/12081910
10. J. de Oliveira Carneiro Brum, T.C. França, S.R. LaPlante and J.D. Villar, *Mini Rev. Med. Chem.*, **20**, 342 (2020); https://doi.org/10.2174/1389557519666191014142448
11. K. Vasantha, G. Basavarajaswamy, M. Vaishali Rai, P. Boja, V.R. Pai, N. Shruthi and M. Bhat, *Bioorg. Med. Chem. Lett.*, **25**, 1420 (2015); https://doi.org/10.1016/j.bmcl.2015.02.043
12. J.M. dos Santos Filho, T.S. Macedo, H.M. Teixeira, D.R. Moreira, S. Challal, J.L. Wolfender, E.F. Queiroz, M.B. Soares, *Bioorg. Med. Chem.*, **24**, 5693 (2016); https://doi.org/10.1016/j.bmc.2016.09.013
13. H. Ünver, B. Berber, R. Demirel and A.T. Koparal, *Anticancer. Agents Med. Chem.*, **19**, 1658 (2019); https://doi.org/10.2174/1871520619666190318125824
14. M. Carcelli, D. Rogolino, A. Gatti, L. De Luca, M. Sechi, G. Kumar, S.W. White, A. Stevaert and L. Naesens, *Sci. Rep.*, **6**, 31500 (2016); https://doi.org/10.1038/srep31500
15. O.I. El-Sabbagh and H.M. Rady, *Eur. J. Med. Chem.*, **9**, 3680 (2009); https://doi.org/10.1016/j.ejmech.2009.04.001
16. C.A. Fraga and E.J. Barreiro, *Curr. Med. Chem.*, **13**, 167 (2006); https://doi.org/10.2174/092986706775197881
17. K. Karrouchi, S. Fettach, M.M. Jotani, A. Sagaama, H.A. Ghabbour, S. Radi, Y.N. Mabkhot, B. Himmi, M. El Abbes Faouzi and N. Issaoui, *J. Mol. Struct.*, **1221**, 128800 (2020); https://doi.org/10.1016/j.molstruc.2020.128800
18. C.M. Leal, S.L. Pereira, A.E. Kümmerle, D.M. Leal, R. Tesch, C.M. de Sant'Anna, C.A. Fraga, E.J. Barreiro, R.T. Sudo and G. Zapata-Sudo, *Eur. J. Med. Chem.*, **55**, 49 (2012); https://doi.org/10.1016/j.ejmech.2012.06.056
19. Y. Liu, B. Lu, J. Lu, C. Xin, J. Li, J. Mu and X. Bao, *Chem. Res. Chin. Univ.*, **29**, 449 (2013); https://doi.org/10.1007/s40242-013-2491-2
20. X.D. Yang, *J. Chem. Res.*, **2008**, 489 (2008); https://doi.org/10.3184/030823408X340799
21. M. Xing, T.T. Zhao, Y.J. Ren, N.N. Peng, X.H. Yang, X. Li, H. Zhang, G.Q. Liu, L.R. Zhang and H.L. Zhu, *Med. Chem. Res.*, **23**, 3274 (2014); https://doi.org/10.1007/s00044-014-0909-0
22. D. Kaushik, S.A. Khan, G. Chawla and S. Kumar, *Eur. J. Med. Chem.*, **45**, 3943 (2010); https://doi.org/10.1016/j.ejmech.2010.05.049
23. M.A.-A. El-Sayed, N.I. Abdel-Aziz, A.A.-M. Abdel-Aziz, A.S. El-Azab, Y.A. Asiri and K.E.H. ElTahir, *Bioorg. Med. Chem.*, **19**, 3416 (2011); https://doi.org/10.1016/j.bmc.2011.04.027
24. A.G.M. Fraga, C.R. Rodrigues, A.L.P. de Miranda, E.J. Barreiro and C.A.M. Fraga, *Eur. J. Pharm. Sci.*, **11**, 285 (2000); https://doi.org/10.1016/S0928-0987(00)00102-0
25. J. Davies and D. Davies, *Microbiol. Mol. Biol. Rev.*, **74**, 417 (2010); https://doi.org/10.1128/MMBR.00016-10
26. G.M. Rossolini, F. Arena, P. Pecile and S. Pollini, *Curr. Opin. Pharmacol.*, **18**, 56 (2014); https://doi.org/10.1016/j.coph.2014.09.006
27. R.J. Fair and Y. Tor, *Perspect. Med. Chem.*, **6**, 25 (2014); https://doi.org/10.4137/PMC.S14459
28. K. Papenfort and B. Bassler, *Nat. Rev. Microbiol.*, **14**, 576 (2016); https://doi.org/10.1038/nrmicro.2016.89
29. A. Deep, U. Chaudhary and V. Gupta, *J. Lab. Physicians*, **3**, 4 (2011); https://doi.org/10.4103/0974-2727.78553
30. G. Cheng, M. Dai, S. Ahmed, H. Hao, X. Wang and Z. Yuan, *Front. Microbiol.*, **7**, 470 (2016); https://doi.org/10.3389/fmicb.2016.00470
31. M. Gajdács and G. Spengler, *Antibiotics*, **8**, 270 (2019); https://doi.org/10.3390/antibiotics8040270
32. R. Sathyanarayana, S.K. Bajire, B. Poojary, R.P. Shastry, V. Kumar and R.B. Chandrashekarappa, *J. Iran. Chem. Soc.*, **18**, 1051 (2021); https://doi.org/10.1007/s13738-020-02093-9
33. R.P. Shastry, S.D. Ghate, B. Sukesh Kumar, B.S. Srinath and V. Kumar, *Nat. Prod. Res.*, (2021); https://doi.org/10.1080/14786419.2021.1887866
34. M. Bhat, B. Poojary, B.S. Kalal, P.M. Gurubasavaraja Swamy, S. Kabilan, V. Kumar, N. Shruthi, S.A. Alias Anand and V.R. Pai, *Future Med. Chem.*, **10**, 1017 (2018); https://doi.org/10.4155/fmc-2017-0191
35. N. Kumar, S. Sreenivasa, A. Prashanth, V. Kumar, V. Chandramohan, B.S. Holla, P. Vishwantha and A.K. Yadav, *Chem. Data Collect*, **32**, 100665 (2021); https://doi.org/10.1016/j.cdc.2021.100665
36. SAINT Plus, Data Reduction Software, version 7.34 a. Bruker AXS Inc.: Madison, WI (2005).
37. G.M. Sheldrick, *Acta Crystallogr. C*, **71**, 3 (2015); https://doi.org/10.1107/S2053229614024218
38. A.L. Spek, *J. Appl. Cryst.*, **36**, 7 (2003); https://doi.org/10.1107/S0021889802022112
39. C.F. Macrae, I.J. Bruno, J.A. Chisholm, P.R. Edgington, P. McCabe, E. Pidcock, L. Rodriguez-Monge, R. Taylor, J. van de Streek and P.A. Wood, *J. Appl. Cryst.*, **41**, 466 (2008); https://doi.org/10.1107/S0021889807067908
40. S.K. Wolff, D.J. Grimwood, J.J. McKinnon, M.J. Turner, D. Jayatilaka and M.A. Spackman, Crystal Explorer (Version 3.1). University of Western Australia (2012).
41. C.F. Mackenzie, P.R. Spackman, D. Jayatilaka and M.A. Spackman, *IUCrJ*, **4**, 575 (2017); https://doi.org/10.1107/S205225251700848X
42. S. Madan Kumar, B.C. Hemraju, S.M. Anil, N.K. Manjunatha, M.T. Swamy, N.K. Lokanath, M. Al-Ghorbani, N. Al-Zaqri and A. Alsalme, *Z. Kristallogr. Cryst. Mater.*, **235**, 85 (2020); https://doi.org/10.1515/zkri-2019-0065

43. H.M. Mahesha Krishnegowda, C.S. Karthik, P.J. Kudigana, P. Mallu and L.K. Neratur, *Polyhedron*, **185**, 114571 (2020); https://doi.org/10.1016/j.poly.2020.114571
44. M.J. Frisch, G.W. Trucks, H.B. Schlegel, G.E. Scuseria, M.A. Robb, J.R. Cheeseman, G. Scalmani, V. Barone, G.A. Petersson, H. Nakatsuji, X. Li, M. Caricato, A.V. Marenich, J. Bloino, B.G. Janesko, R. Gomperts, B. Mennucci, H.P. Hratchian, J.V. Ortiz, A.F. Izmaylov, J.L. Sonnenberg, D. Williams-Young, F. Ding, F. Lipparini, F. Egidi, J. Goings, B. Peng, A. Petrone, T. Henderson, D. Ranasinghe, V.G. Zakrzewski, J. Gao, N. Rega, G. Zheng, W. Liang, M. Hada, M. Ehara, K. Toyota, R. Fukuda, J. Hasegawa, M. Ishida, T. Nakajima, Y. Honda, O. Kitao, H. Nakai, T. Vreven, K. Throssell, J.A. Montgomery Jr., J.E. Peralta, F. Ogliaro, M.J. Bearpark, J.J. Heyd, E.N. Brothers, K.N. Kudin, V.N. Staroverov, T.A. Keith, R. Kobayashi, J. Normand, K. Raghavachari, A.P. Rendell, J. C. Burant, S.S. Iyengar, J. Tomasi, M. Cossi, J.M. Millam, M. Klene, C. Adamo, R. Cammi, J.W. Ochterski, R.L. Martin, K. Morokuma, O. Farkas, J.B. Foresman and D.J. Fox, Gaussian, Inc., Wallingford CT, Gaussian 16, Revision C.01 (2016).
45. B. Civalleri, C.M. Zicovich-Wilson, L. Valenzano and P. Ugliengo, *CrystEngComm*, **10**, 405 (2008); https://doi.org/10.1039/B715018K
46. R. Dennington, T. Keith and J. Millam, GaussView, Version 6.1, Semichem Inc., Shawnee Mission, KS (2016).
47. R.P. Shastry, P.D. Rekha and V.R. Rai, *Biocatal. Agric. Biotechnol.*, **18**, 101009 (2019); https://doi.org/10.1016/j.bcab.2019.01.047
48. J.H. Choo, Y. Rukayadi and J.K. Hwang, *Lett. Appl. Microbiol.*, **42**, 637 (2006); https://doi.org/10.1111/j.1472-765X.2006.01928.x
49. H. Zhu, C.C. He and Q.H. Chu, *Lett. Appl. Microbiol.*, **52**, 269 (2011); https://doi.org/10.1111/j.1472-765X.2010.02993.x
50. P.S. Rajesh and V.R. Rai, *Microbiol. Res.*, **169**, 561 (2014); https://doi.org/10.1016/j.micres.2013.10.005
51. Mahesha, T.C. Raveesha, M.K. Hema, P.G. Chandrashekara, K.J. Pampa, K. Mantelingu, T. Demappa and N.K. Lokanath, *J. Mol. Struct.*, **1225**, 129104 (2021); https://doi.org/10.1016/j.molstruc.2020.129104
52. S.M. Kumar, V. Kumar, M. Al-Ghorbani, B.S. Holla, B. Poojary, P. Praveen, S.C. Nayak, J.S. Mohan, S. Thamotharan, V.R. Shamprasad, N.K. Lokanath, N. Al-Zaqri and A. Alsalme, *Z. Kristallogr. Cryst. Mater.*, **235**, 569 (2020); https://doi.org/10.1515/zkri-2020-0052